Magnetic Resonance Imaging 39 (2017) 168–174

Contents lists available at ScienceDirect

Magnetic Resonance Imaging

journal homepage: www.mrijournal.com

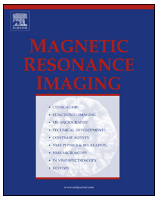

Original contribution

Quantifying the dynamic density driven convection in high permeability packed beds

Ying Teng [a], Lanlan Jiang [a,b,*], Yingting Fan [a], Yu Liu [a], Dayong Wang [a], Abuliti Abudula [c], Yongchen Song [a]

[a] *Key Laboratory of Ocean Energy Utilization and Energy Conservation of Ministry of Education, Dalian University of Technology, 116024 Dalian, China*
[b] *Research Institute of Innovative Technology for the Earth, Kizugawa City, Kyoto 619-0292, Japan*
[c] *North Japan New Energy Research Center, Hirosaki University, Aomori City 0300831, Japan*

ARTICLE INFO

Article history:
Received 15 February 2017
Received in revised form 9 March 2017
Accepted 11 March 2017
Available online xxxx

Keywords:
Density driven convection
Finger growth regimes
Onset time
Mixing time
Rayleigh number

ABSTRACT

The density driven convection phenomenon is expected to have a significant and positive role in CO_2 geological storage capacity and safety. The onset and development of density-driven convective on the core scale is critical to understand the mass transfer mechanism. In this paper, laboratory experiments were conducted to investigate the density-driven convective in a vertical tube. The deuterium oxide (D_2O)/manganese chloride ($MnCl_2$) water solution in water or brine were as an analog for CO_2-rich brine in original brine. Experiments are repeated with variations in permeability to vary the characteristic Rayleigh number. Based on the MRI technology, the intensity images showed the interface clearly, reflecting the transition from diffusion to convective. With the echo-multi-slice pulse sequence method, the intensity images can be obtained as 2 min 8 s. For the denser fluid pairs, fingers appeared, propagated, coalesced and multi-fingers formed. The finger growth rate of the convective was visualized as three distinct periods: rising, stable and declining. Detailed information regarding the wave number, wave length, onset time and mixing time as functions of Rayleigh number are developed.

1. Introduction

Carbon capture and sequestration (CCS) is expected to play a major role in meeting CO_2 emission reduction targets [1]. The injected CO_2 formed a thin layer of free phase below the caprock; and then the above CO_2 dissolve in the brine by molecular diffusion creates a dense boundary layer of CO_2-rich brine in comparison to CO_2-poor brine densities [2]. The density of the boundary layer at the interface is 0.1–1% denser than the original brine, depending the on pressure, temperature and salinity [3]. Due to the gravitational instability, a pattern of the downward flow of CO_2-rich brine that looks like fingers will appear, referring to as convective fingers [4]. In contrast to molecular diffusive dissolution, the so-called density-driven natural convection significantly increases the rate of CO_2 dissolution, reduces time for dissolution trapping and enhances the safety of the storage in the saline aquifer [5].

Density-driven natural convection has received increasing attention both from theoretical [6,7] and experimental [8,9] point of view. The earliest report [10] investigated density-driven natural convection effect on CO_2 dissolution, and then the convection stability criteria for vertical flow that subjected to both thermal and density gradients [11] and for onset time in the anisotropic porous media [12]. Besides of the numerical study, several laboratory scale experiments were conducted to analyze convective dissolution by using Hele-Shaw cell [8]; [13–15], and the convective mixing process with optical techniques, such as a Schlieren technique [16] and or holographic interferometry [17]. These technology of Hele-Shaw cell provides visualization for convective fingers propagate, however, only mathematically analogous to flow in porous media [18] and limited at ambient conditions [19]. Then the amount of CO_2 dissolved into solution, bulk dissolution rate and the onset of the density-driven convection were also investigate at high pressure by using mercury-free DBR pressure-volume temperature (PVT) [20], stainless-steel cylindrical blind cell [2,21] by monitoring pressure decay. The results showed the mass transfer rate was usually larger than expected from a diffusion process alone. Those experiments cannot provide visual observation of occurrence of convective and the instabilities because of using blind cell.

The dimensionless parameter Rayleigh number (*Ra*), nominally expresses the ratio of convective and diffusive transport in the natural convection process [22]. The density-driven natural convection is expected for Rayleigh number above $4\pi^2$ in porous media [23]. While the mass transfer or convective flux [19], the onset time of convective currents [24], the critical wave length and the wave numbers of the finger [25] are all as functions of the Rayleigh number in the range of

---

[*] Corresponding author at: Key Laboratory of Ocean Energy Utilization and Energy Conservation of Ministry of Education, Dalian University of Technology, 116024 Dalian, China.

E-mail address: lanlan@dlut.edu.cn (L. Jiang).

http://dx.doi.org/10.1016/j.mri.2017.03.004
0730-725X/© 2017 Elsevier Inc. All rights reserved.

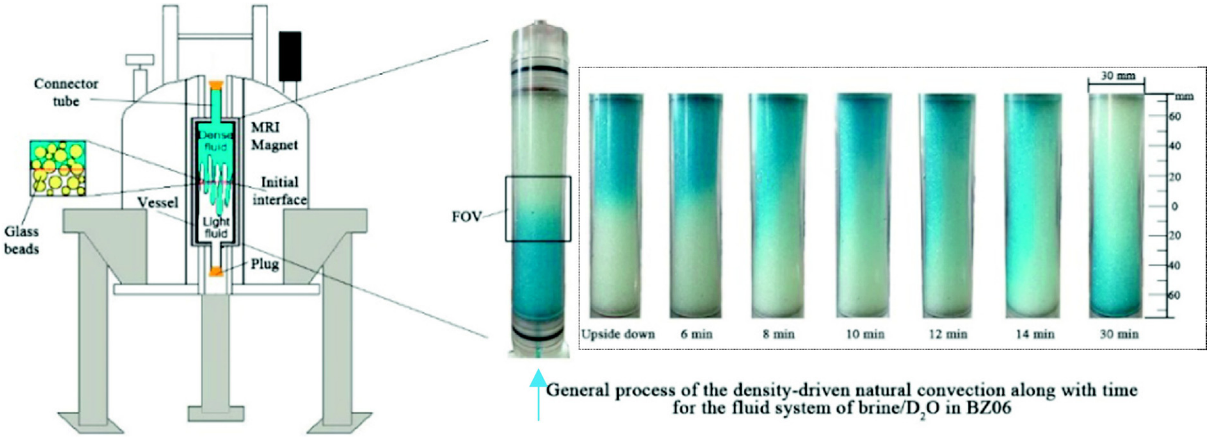

Fig. 1. Schematic diagram of the experimental setup. Left shows the MRI experimental machine with the connector tube. Right shows the convection for one fluid pair in BZ-06. Denser fluid was injected from the bottom and indicted with blue color. (For interpretation of the references to color in this figure legend, the reader is referred to the web version of this article.)

5000–30,000 [26], with similar conditions in real saline aquifers, due to the different properties of porous media [27]. The visual observation for investigating the finger growth regime of convection mixing is particularly important. With the development of the visualization and surface measurement techniques, X-ray computed tomography (CT) [28] and Magnetic Resonance Image (MRI) are the available experimental methods to observe multiphase flow behavior in porous media [29]. MRI technology has the advantage of nondestructive visualizing the fluid distribution during fluid flow in porous media [30].

Up to date, few studies was conducted to experimental investigate the density-driven natural convection process in porous media. In this paper, we visualized the density-driven natural convection in porous media by using MRI. The development of convective fingers was investigated, and the quantitative analysis of the finger growth rates, the wave numbers, the initial wave length, the convection onset time and mixing time were achieved. And then we discussed the effect of Rayleigh number on the wave number, wave length and convection time. Such investigation aid in conceptual understanding of the density-driven natural convection and help inform studies for CO_2 sequestration in saline aquifers.

2. Experimental methods

2.1. Experimental apparatus and material

The schematic diagram of the experimental setup is shown in Fig. 1, including a high-resolution MRI machine for images acquisition, and a vessel for porous media. The Varian 400 MHz NMR system (Varian Inc., Palo Alto, CA, USA), 9.4 T magnet, was used for Proton (^1H) images acquired. Pack sand was contained in a vessel with 150-mm length, 30-mm internal diameter. The vessel was made from melamine resin which did not affect the magnetic signals during measurement and was transparent to monitor outside MRI system as shown in Fig. 1. After degassing step in a Nalgene transparent polycarbonate desiccator (5311-0250, Thermo Scientific, Waltham, MA, USA) using a vacuum pump (Edwards, model E2M1.5), fluid was injected into the porous media by using an accurate syringe pump (Chin-Fin Technology, LC 3060).

Four kinds of porous media were packed with plastic sands (US1, 250–425 μm in diameter, 337.5 μm in average diameter, Ube Sand Engineering Co. Ltd., XH40/60), and glass beads (BZ02, 150–250 μm, 200 μm in average diameter; BZ04, 350–450 μm, 400 μm in average diameter; BZ06, 550–650 μm, 600 μm in average diameter, As-One Co. Ltd., Japan).

Three different kinds of fluid pairs: H_2O/D_2O, brine/D_2O and $H_2O/MnCl_2$ were used.D_2O with a stated purity of 99.9% and the $MnCl_2$ water solution were used as the denser fluids; deionized water or brine was used as the light fluid. The additive of coloured dye Bromocresol green (0.05%) was added into the lighter fluid to allow visual monitoring of flow and transport before MRI experiments. The properties of the porous media .i.e., porosity and permeability, and fluids were list in Table 1.

Deionized water (H_2O) and brine could be determined from the measured MRI intensities because ^1H; However, deuterium oxide (D_2O) does not emit an MR signal. The additive paramagnetic ion, such as Mn^{2+}, can reduce the relaxation time [31] and thereby the $MnCl_2$ water solution is invisible in the MRI images. In other words, for the fluids system of H_2O/D_2O and brine/D_2O, we can distinguish between ^1H and D; for the fluid system of $H_2O/MnCl_2$, we can make a distinction between H_2O and $MnCl_2$ solution.

2.2. Experimental procedure

After leakage check under the certain pressure, the vessel was filled with packed porous media. The light fluid (H_2O or brine) was injected to

Table 1
Parameters of fluids and porous media in experiments.

Case	Fluid pair	Porous media	Porosity	Permeability	Density difference (kg/m^3)	Viscosity (Pa·s)	Diffusion coefficient (m^2/s)	*Ra*
A	H_2O/D_2O	US1	0.354	28.63	0.1	0.914	2×10^{-9}	320.803
B	Brine/D_2O				0.05	0.914	1.7×10^{-9}	188.707
C	$H_2O/MnCl_2$				0.1	1.62	1.04×10^{-9}	349.076
D	H_2O/D_2O	BZ-02	0.48	57.1	0.1	0.914	2×10^{-9}	471.928
E	Brine/D_2O				0.05	0.914	1.7×10^{-9}	277.605
F	$H_2O/MnCl_2$				0.1	1.62	1.04×10^{-9}	513.521
G	H_2O/D_2O	BZ-04	0.398	64.64	0.1	0.914	2×10^{-9}	644.253
H	Brine/D_2O				0.05	0.914	1.7×10^{-9}	378.972
I	$H_2O/MnCl_2$				0.1	1.62	1.04×10^{-9}	701.033
J	H_2O/D_2O	BZ-06	0.431	111.58	0.1	0.914	2×10^{-9}	1027.05
K	Brine/D_2O				0.05	0.914	1.7×10^{-9}	604.150
L	$H_2O/MnCl_2$				0.1	1.62	1.04×10^{-9}	1117.574